Toward enhanced quality assurance guidelines for deep hyperthermia devices: a multi-institution study

International Journal of Hyperthermia

ISSN: (Print) (Online) Journal homepage: www.tandfonline.com/journals/ihyt20

Toward enhanced quality assurance guidelines for deep hyperthermia devices: a multi-institution study

Mattia De Lazzari, Carolina Carrapiço-Seabra, Dietmar Marder, Gerard C. van Rhoon, Sergio Curto & Hana Dobšíček Trefná

To cite this article: Mattia De Lazzari, Carolina Carrapiço-Seabra, Dietmar Marder, Gerard C. van Rhoon, Sergio Curto & Hana Dobšíček Trefná (2024) Toward enhanced quality assurance guidelines for deep hyperthermia devices: a multi-institution study, International Journal of Hyperthermia, 41:1, 2436005, DOI: 10.1080/02656736.2024.2436005

To link to this article: https://doi.org/10.1080/02656736.2024.2436005

INTERNATIONAL JOURNAL OF HYPERTHERMIA
2024, VOL. 41, NO. 1, 2436005
https://doi.org/10.1080/02656736.2024.2436005

Toward enhanced quality assurance guidelines for deep hyperthermia devices: a multi-institution study

Mattia De Lazzari[a*], Carolina Carrapiço-Seabra[b*], Dietmar Marder[c], Gerard C. van Rhoon[b,d], Sergio Curto[b†] and Hana Dobšíček Trefná[a†]

[a]Department of Electrical Engineering, Chalmers University of Technology, Gothenburg, Sweden; [b]Department of Radiotherapy, Erasmus MC Cancer Institute, University Medical Center Rotterdam, Rotterdam, The Netherlands; [c]Center for Radiation Oncology KSA-KSB, Cantonal Hospital Aarau, Aarau, Switzerland; [d]Department of Radiation Science and Technology, Delft University of Technology, Faculty of Applied Sciences, Delft, The Netherlands

ABSTRACT

Introduction: Hyperthermia efficacy depends on the temperatures achieved in the target area. Therefore, hyperthermia systems must deliver both controlled and conformal heating. This study presents a comprehensive multi-institutional quality assurance (QA) evaluation of deep hyperthermia devices.

Methods: Six European institutions equipped with BSD- Sigma 60 and Sigma Eye deep hyperthermia applicators participated in the study. Up to six measurements per applicator were performed in each institution. The thermal distribution in cylindrical homogeneous phantoms after 10 minutes of heating with a total power delivered of 1000 watts was assessed using the applicator's integrated mapping thermometry system. Evaluated quality parameters included temperature increase, focus location, and focus symmetry.

Results: A total of 54 measurements were conducted, with 43 included in the analysis. All applicators, except one, achieved a temperature increase of 6 °C in 10 minutes. Central heating capabilities were demonstrated, with mean deviations from the intended location of −1.4 ± 1.6 cm for Sigma 60 and 1.5 ± 1.4 cm for Sigma Eye. Symmetry evaluations showed differences in radial temperature profiles of 6.2 ± 4.5 % for the Sigma 60 and 5.9 ± 4.4 % for the Sigma Eye. We propose minimum acceptable values for each quality parameter based on these results.

Conclusion: The measurements were reproducible with acceptable values for the various quality parameters. Potential deviations might be attributed to inaccuracies in the mapping thermometry system rather than the heating system. The presented protocol and practical recommendations should be applied for future QA measurements in deep hyperthermia.

ARTICLE HISTORY
Received 13 August 2024
Revised 11 October 2024
Accepted 25 November 2024

KEYWORDS
Hyperthermia; quality assurance; deep hyperthermia applicators; homogeneous phantom; measurement protocol

1. Introduction

Hyperthermia is a cancer treatment designed to increase target temperatures to 39–44 °C for 60–90 minutes. When combined with radiotherapy and/or chemotherapy, hyperthermia acts as a powerful biological sensitizer, significantly enhancing the effectiveness of these treatments [1,2]. Numerous studies have demonstrated enhanced therapeutic outcomes with the addition of hyperthermia, resulting in improved local tumor control and survival rates, without increasing toxicity [3–10]. Moreover, promising results have been observed when combining hyperthermia with immunotherapy [11]. Studies examining the dose-response relationship in hyperthermia have highlighted the importance of achieving high thermal doses during treatment [12–14]. This implies that hyperthermia systems should be able to deliver selective and controlled heating to a predefined target volume while minimizing heat exposure to surrounding healthy tissues. To ensure these criteria are met, quality assurance (QA) guidelines have been developed and refined over the years.

Numerous authors contributed to establishing guidelines for hyperthermia devices. Dewhirst et al. [15] provided QA recommendations for multi-institutional trials, with a strong focus on thermometry and related aspects. Lagendijk et al. [16] drew on the collective expertise of institutes involved in successful clinical trials to propose comprehensive guidelines, covering various stages of the hyperthermia workflow, from treatment planning to delivery and documentation. Building on these contributions, Bruggmoser et al. [17,18] focused on the specifics of deep hyperthermia devices, offering QA guidelines tailored to loco-regional and deep treatments.

CONTACT Mattia De Lazzari lazzari@chalmers.se Department of Electrical Engineering, Chalmers University of Technology, Gothenburg, Sweden
*Shared first authorship
†Shared last authorship

Supplemental data for this article can be accessed online at https://doi.org/10.1080/02656736.2024.2436005.

These encompass QA aspects across the clinical application of hyperthermia, including indication, preparation, treatment, and standardized analysis. Recent contributions by Dobsicek Trefna et al. expanded the existing guidelines, offering additional QA recommendations covering specific treatment modalities, namely superficial [19,20] and interstitial [21] hyperthermia. Currently, the European Society for Hyperthermic Oncology (ESHO) Technical Committee is revising the guidelines for deep hyperthermia (manuscript in preparation), with the most significant modification being the inclusion of temperature-based quality parameters. The key requirement is a minimum temperature increase of 6 °C in 10 min, achieved in a homogeneous tissue-mimicking phantom. This criterion is based on a study by Wust et al. [22], who found that a specific absorption rate (SAR) of 13 W/kg was required to produce a 6 °C temperature increase in a phantom within 30 minutes. More recent studies confirmed this finding, showing that clinical devices could achieve a 6 °C increase when applying a power output of 1000 watts [23,24].

Characterizing deep hyperthermia devices based on temperature, using the system's own thermometry probes, poses several challenges. Monitoring temperature comprehensively over clinically significant areas is challenging due to the limited number of thermal probes available for each applicator. In essence, accurately translating a limited number of carefully selected temperature measurement points to three-dimensional (3D) temperature distributions is fundamental, yet not straightforward [24]. Moreover, the accuracy of these measurements heavily relies on each temperature being measured at the designated location. This necessitates the use of well-designed phantoms with fixed and known catheter positioning and protocols with parameters that can be obtained from such measurements and phantoms. Developing experimental expertise is imperative to accumulate the knowledge required for establishing updated QA guidelines for deep hyperthermia devices applicable across all hyperthermia institutions.

This study outlines the experimental design, practical implementation, and analysis of phantom measurements for deep hyperthermia devices. The study aims to gather information on practical implementation regarding system set-up and required time to perform the QA protocol. Ultimately, the study offers crucial insights that can be translated as recommendations for the forthcoming deep hyperthermia QA guidelines. Measurements were carried out across six different European institutions where clinical hyperthermia is practiced, being the largest multi-institution QA study conducted in hyperthermia to date. We specifically investigated the performance of the BSD-Sigma 60 and BSD-Sigma Eye applicators (Pyrexar Medical, Salt Lake City, Utah, United States) installed at the University Hospitals of Berlin, Düsseldorf, Erlangen, Munich, and Tübingen in Germany, as well as at the Erasmus Medical Center Cancer Institute in Rotterdam, The Netherlands. All the involved centers have over 20 years of experience in applying hyperthermia treatments clinically.

2. Materials and methods

A new part of the upcoming QA guidelines is that temperature readings are taken using the existing thermometry systems at each institution, following standard clinical practices. Our objective was to assess temperature distribution within the tissue-mimicking phantoms after a 10-minute heating period, utilizing a consistent total forwarded power of 1000 watts for each device under evaluation.

The data collection phase spanned approximately three weeks, with two days allocated to each institution. We planned three repetitions of each heating experiment, maintaining the same parameters throughout to ensure reproducibility. Measurement days were meticulously scheduled in advance to avoid conflicts with ongoing clinical treatments. However, some unavoidable scheduling overlaps occurred. Consequently, on those days, six measurements were not achievable at some institutions. Three identical tissue-mimicking phantoms were used, enabling six experiments daily, split evenly between morning and afternoon sessions. Following each experiment, there was a mandatory five-hour interval to allow the phantoms to return to room temperature, ensuring consistent conditions for subsequent tests. To ensure consistency, we limited each phantom to two measurements per day. Before and after daily measurements, the phantoms were acclimated to the temperature of the clinical room where the measurements were conducted.

2.1. QA phantom design

The deep hyperthermia measurements were conducted using three identical, homogeneous tissue-mimicking phantoms. Figure 1 shows a three-dimensional (3D) representation of the phantom design. More detailed measures are provided in the Supplementary Materials (Figures S1–S3). Each phantom featured an external cylindrical PVC shell with a thickness of 0.8 cm and an outer diameter of 25 cm, sealed with two watertight lids, each located at 30 cm from the phantom center, making them 60 cm apart. Each phantom was equipped with 16 6 F catheters to house temperature probes: 14 longitudinal catheters aligned with the vertical direction of the phantom (z-axis) and two radial catheters placed perpendicularly to the longitudinal catheters (x-y plane). The longitudinal catheters measured 30 cm, reaching the central plane of the phantom. Of the 14 longitudinal catheters, 13 were accessible from one of the two lids enclosing the phantom and placed along the x- and y-axes, spaced 3 cm apart. The two radial catheters intersected at the central plane of the phantom, forming a 90° angle. These two radial catheters will be referred to as radial catheters R1 and R2. The position of the catheters inside the phantom was maintained by using eight equispaced 3D-printed annular structures. A smaller double 3D-printed ring structure was used to hold the position of the two radial catheters. The closed tip of each radial catheter was securely attached to the PVC shell using water-resistant adhesive.

The phantom was filled with approximately 30 L of Perfax powder wallpaper paste-based tissue-mimicking solution, prepared by mixing deionized water with 3.5 g/L of sodium chloride and 40 g/L of Perfax powder (Henkel, Düsseldorf, Germany). The mixture was manually prepared in 3-liter batches to maintain consistency and ensure a uniform mixing process. Each batch was mixed for about 5 minutes,

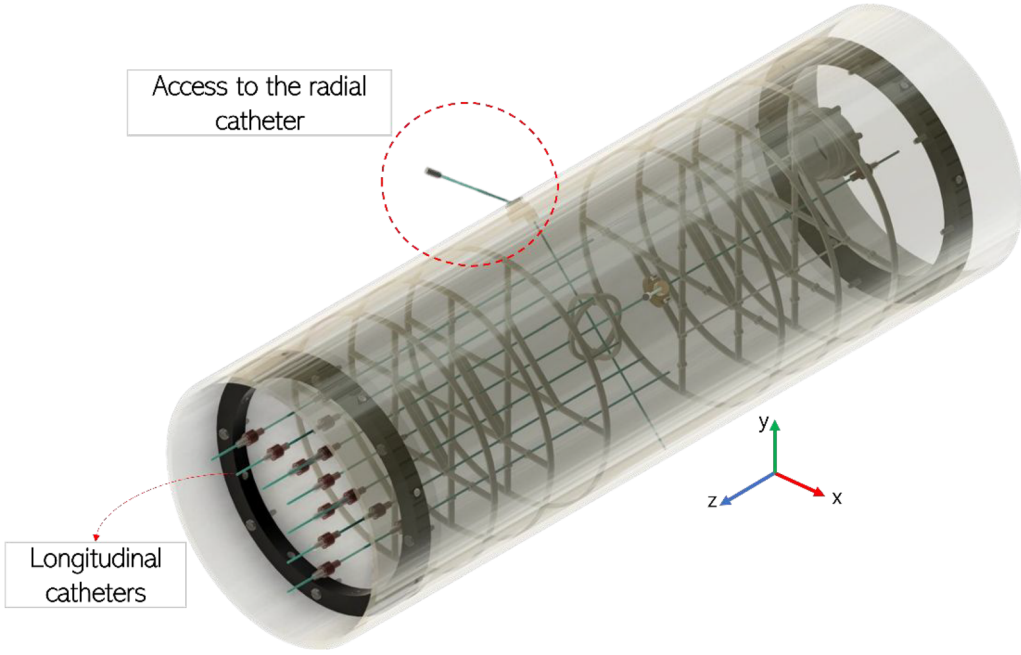

Figure 1. Schematic 3D representation of the phantom used in the measurements. It illustrates the cylindrical PVC shell, the catheters, and the corresponding 3D-printed annular structures that secure the catheters. Longitudinal catheters were positioned along the z-axis, while the two radial catheters were placed in the x-y plane, intersecting the z-axis at the center of the cylinder.

before being poured into the phantom shell. After filling, the phantom shells were left with the lid open overnight to allow air bubbles to escape. The average total weight of each phantom was 32.6 ± 0.1 kg, confirming uniformity across the phantoms.

2.2. Phantom properties characterization

Dielectric properties of the wallpaper paste-based tissue-mimicking solution were measured following the methodology outlined by La Gioia et al. [25]. The dielectric properties evaluation was performed using an open-ended coaxial probe (DAK 12, Schmid & Partner Engineering AG, Zurich, Switzerland) connected to a two-port Rohde & Schwarz ZNC 3 VNA. Measurements were conducted at room temperature (21 °C) over the 10 – 500 MHz frequency range, with a resolution of 1 MHz. The probe underwent calibration through an open-short-load routine, utilizing distilled water at room temperature as load material. Calibration accuracy was further validated by measuring a saline solution with known properties. Then, ten batches of the tissue-mimicking solution were measured, and final values of permittivity (ε_r) and conductivity (σ) were calculated as the averages of these different batches.

The thermal properties of the tissue-mimicking solution, namely thermal conductivity (k) and volumetric heat capacity (c), were also assessed. For this purpose, a commercial thermal analyzer (TEMPOS, Meter Group, Inc., Pullman, WA, USA, accuracy: ±10%) with the dual-needle sensor (SH-3) was used. Measurements were based on the hot wire technique: heat was transferred from one needle for 30 s to the surrounding tissue. The second needle recorded the consequent temperature increase for 90 s, and the device derived thermal properties, as described by Silva et al. [26,27]. The final thermal properties values were calculated as averages from ten different batches of phantom material.

Previous studies have demonstrated the stability of this phantom mixture over time [27]. Therefore, we assumed the properties of the phantom to be constant throughout all the measurements, as the material was stored at room temperature and shielded from external contaminants.

2.3. QA measurement protocol

All experiments were conducted in the BSD-2000, using the Sigma 60 and the Sigma Eye phased array applicators (Pyrexar Medical, Salt Lake City, USA). The BSD-2000 Sigma 60 operates at frequencies between 75 and 100 MHz and features an array of eight equispaced dipoles enclosed within a cylindrical-shaped transparent plastic shell featuring an external diameter of 60 cm. The BSD-2000 3D Sigma Eye operates at 100 MHz and consists of 24 identical dipole antennas distributed across three eye-shaped rings, each containing eight antennas [28].

For each applicator, six measurements were planned: three with a centric target and three with an eccentric target. Temperatures inside the phantom were assessed using each institution's thermal probes (single-sensor thermistors). The thermal probes were integrated with a thermal mapping system capable of mapping temperature distribution along the different catheters. This is achieved by mechanically retracting the probe from its initial position (fully inserted in the catheter) to the final position with a user-defined step size. The step size utilized for probe retraction was 0.5 cm, with a maximum mapping length of 25 cm. Due to the variability in the number of probes available in the different institutes, we required a minimum of

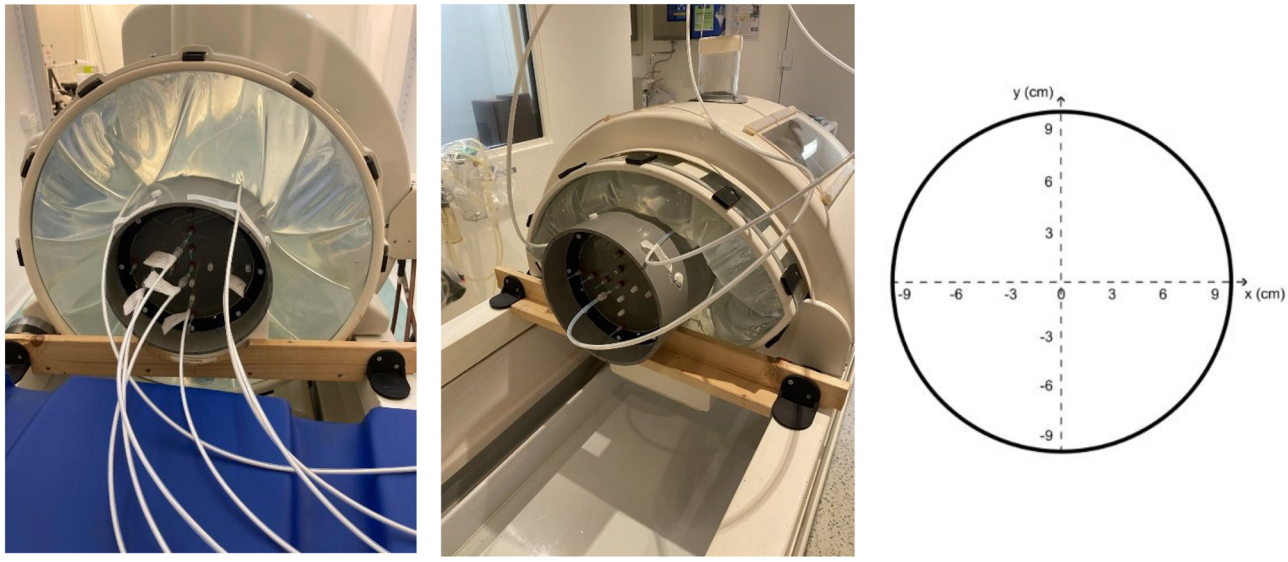

Figure 2. The final experimental setups for the Sigma 60 (a) and Sigma Eye (b) applicators are shown. The coordinate reference system is depicted in (c). The custom-made wooden supports, used to maintain the phantom vertical position, are also visible in (a) and (b).

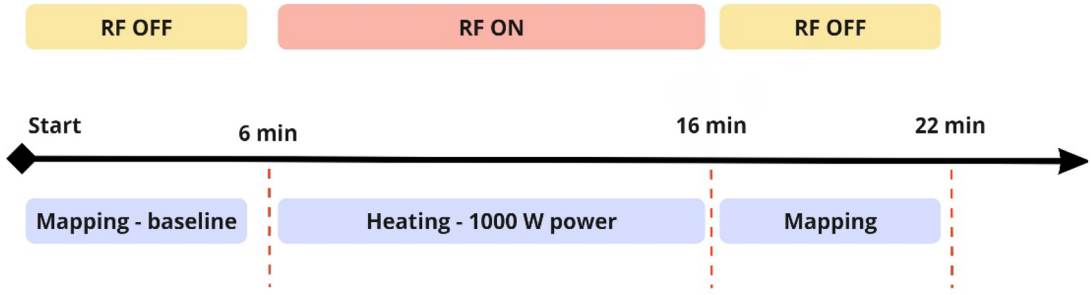

Figure 3. The measurement scheme for a single phantom experiment is outlined. Each temperature mapping procedure lasted 6 minutes, covering a mapping length of 25 cm and a step size of 0.5 cm. (RF: radiofrequency).

three thermal mapping probes. Two of these probes were inserted in the radial catheters, enabling the analysis of temperature distribution on the central x-y plane of the phantom. Another probe was inserted in the longitudinal catheter positioned at the focus location.

Before starting the measurement, the phantom was carefully positioned in the applicator using custom-made wooden supports. This ensured a centered positioning within the applicator aperture (x- y-axes). At one institution (Institution 6), due to the absence of support structures for the Sigma Eye applicator, the phantom was positioned using the patient hammock. To maintain accurate alignment along the longitudinal axis (z-axis), distances between the applicator edge and the phantom edge on both sides were measured and kept equal. The final longitudinal alignment of the phantom was peer-verified. After this procedure, two thermal probes were inserted in the two radial catheters and the bolus was filled. Care was taken while filling the bolus to avoid any movement of the phantom. The remaining probe was inserted in the longitudinal catheter where the focus was located. When more than three thermal probes were available, these were positioned at coordinates (x, y) cm of (6, 0), (0, 6), (-6, 0) and (0, −6). Two examples of the final experimental setups for the Sigma 60 and Sigma Eye applicators are shown in Figure 2.

The same measurement procedure was adopted for all repetitions, as schematically represented in Figure 3. An initial baseline thermal mapping scan was performed with the power off, lasting 6 minutes. Subsequently, power was applied for 10 minutes with a total forward power of 1000 W. At the end of the heating period, a second mapping scan was conducted to record the new temperature profile. Following each measurement, a 5-hour interval was observed before reusing the same phantom to allow its temperature to equilibrate with the room temperature.

2.4. Data analysis

2.4.1. Exclusion criteria

Before proceeding with the data analysis, datasets obtained from each experiment were thoroughly examined for suitability. Experiments were excluded based on the following predefined criteria:

a. Failure in data recording: experiments were excluded if the software failed to save data from one or more thermal mapping repetitions.
b. Failure in the temperature monitoring system: experiments were excluded if temperature data were not recorded on the central longitudinal probe, i.e., the longitudinal probe in the focus location, or on both radial probes. Such instances were considered inadequate for the comprehensive evaluation of quality parameters. However, experiments were not excluded if data from only one of the two radial probes were corrupted.
c. Dominant hotspots: experiments were excluded if dominant hotspots prevented the precise definition of a focal area. In such cases, qualitative verification of the applicator performance using a lamp phantom was necessary.

2.4.2. Quantitative evaluation of the QA measurements

To evaluate the temperature measurements and the heating quality of the used systems, the following quality parameters were analyzed: (1) temperature increase, (2) focus location, (3) focus symmetry. These parameters are described in the following sections. Temperature profiles were calculated by subtracting the baseline mapping scan from the final mapping scan, providing relative temperature increases, rather than absolute temperature values. The analyzed mapping length was 24 cm (from 25 cm) to account for the 0.8 cm catheter passing through phantom shell on the exit. Longitudinal probes mapped from the center toward the lid of the phantom ($z = 0$ cm to $z = 25$ cm). Radial probes mapped along the radius of the phantom, starting at −12 cm, passing through 0 cm and ending at 12 cm.

2.4.2.1. Temperature increase. The maximum temperature increase was evaluated with the longitudinal thermal probe placed in the catheter corresponding to the focus location. For each experiment, the maximum value from the temperature profile of the longitudinal probe at the focus location was taken. Values were averaged across repetitions for each focus location (centric or eccentric), system, and institution.

2.4.2.2. Focus location. For a centric focus location, the data from two radial probes were used. The data points were fitted with an 8th-order polynomial function to identify the location of the maximum temperature. The location of the maximum temperature recorded by each probe was compared to the expected temperature peak location, ideally situated at 12 cm along the mapping track (corresponding to the location 0,0 in the phantom central X-Y plane). This comparison provides an approximate measure of the central focusing ability of each device. This analysis excluded temperature peaks corresponding to hotspots near the phantom wall, when present. These are irrelevant in clinical situations since water circulation in the bolus is performed to avoid hotspots on the skin surface.

2.4.2.3. Focus symmetry. The symmetry of the focal area was assessed on the X-Y plane for the centric target. We used two radial probes and one longitudinal probe at the target location (Method 1 using radial probes). The two radial probes identified the temperature peak locations (excluding temperature peaks resulting from hotspots near the surface, as explained earlier). Then, we identified two temperature points located 4.5 cm away from the peak. This distance was chosen based on the expected focus size, which is a quarter of a wavelength, corresponding to 8.5 cm with our phantom permittivity at 100 MHz. Thus, we considered points halfway between the phantom center and the focus size. Figure S4 illustrates this procedure. Focus symmetry was quantified as the percentage difference between these two temperature values, where perfect symmetry would yield a zero difference. Additionally, we calculated the distance in centimeters between the peak locations for the two probes to validate the consistency of data captured by the radial probes.

Since more probes were available at some institutions, we also used another method (Method 2, using longitudinal probes) for the symmetry assessment. Longitudinal probes were symmetrically positioned around the center of the phantom at coordinates (x, y) cm of (6, 0), (-6, 0), (0, 6), and (0, −6). The temperature differences between these symmetric locations and the phantom center were computed and averaged (see Figure S5 for more details). This method was applied to Institution 2 and Institution 3 and was compared with Method 1. in this case, we used 6 cm instead of 4.5 cm for the radial probes to maintain consistency with the longitudinal probe and ensure a fair comparison.

3. Results

3.1. Phantom properties characterization

The measured density, dielectric, and thermal properties of the muscle-mimicking phantom solution are presented in Table 1. Additionally, Table 1 includes the dielectric and thermal properties of muscle tissue sourced from the IT'IS database [29]. To facilitate comparison, the percentage differences between the measured and IT'IS values were calculated, with all differences remaining below 10% for all parameters except for permittivity (ε_r). Given that the applicators operated at frequencies between 90 and 105 MHz, we calculated that the variation in dielectric properties across this range was between 0.1% and 0.3%, i.e., negligible.

Table 1. Muscle-mimicking phantom properties at 100 MHz, with corresponding uncertainty. Density, dielectric and thermal properties of muscle tissue, taken from the IT'IS database, are also reported. The percentage differences between the measured values and the IT'IS database values are shown in the last row.

	Density [kg/m^3]	Dielectric properties		Thermal properties	
		Permittivity	Conductivity	Volumetric heat capacity	Thermal conductivity
		ε_r [-]	σ [S/m]	c [J/(kg K)]	k [W/(m K)]
Measured	1035.0 ± 3.8	74.4 ± 3.2	0.67 ± 0.04	3091 ± 69	0.451 ± 0.009
IT'IS [30]	1090 ± 55	66 ± 3.3	0.708 ± 0.04	3421 ± 460	0.49 ± 0.04
Δ%	5.0	12.7	5.4	9.7	8.0

3.2. QA measurements

The total number of QA temperature measurements performed for this study is presented in Table 2. It includes the number of measurements per institution, per applicator, and target location. Some institutions – Institutions 3, 4, and 6 – experienced unexpectedly busy clinical programs, which prevented the completion of the six planned measurements per applicator. In contrast, all planned measurements were performed in Institutions 1 and 2.

At Institution 3, three measurements were discarded: one due to a system data-saving failure and two due to mapping probe failure. Mapping inconsistencies were identified in two measurements for the central target in Sigma 60 at Institution 4, leading to their excluded. At Institution 5, the Sigma 60 was unavailable due to temporal malfunction. For the same institution (Sigma Eye), one centric target measurement was excluded due to inconsistencies on the radial probes and one eccentric target measurement due to failure in the thermometry data-saving system. Finally, at Institution 6, two measurements were excluded due to thermometry data-saving issues (Sigma 60) and one due to mapping issues (Sigma Eye).

3.2.1. Quantitative evaluation of the QA measurements

Centric target measurement results for each institution and applicator are shown in Figure 4 (as average and standard deviation). To facilitate comparison, the normalized temperature profiles for Sigma 60 and Sigma Eye are presented in Figure 5, for each of the three probe locations (radial probes R1 and R2, and longitudinal probe). All profiles show a clear focus, approximately at the center of the phantom (12 cm), with some institutions showing hotspots on the sides, close to the phantom walls. Variation within the same institutions and applicator was minimal, indicating reproducible results.

All the selected data were used to compute quantitative parameters, namely temperature increase, for both centric and eccentric targets. Focus location and focus symmetry were evaluated only for centric target. These results are summarized in Table S2 in the Supplementary Materials. The following paragraphs provide a detailed description of the primary findings for each quantitative parameter evaluated.

3.2.1.1. Temperature increase. On average, temperature increases of 8.8 ± 1.2 °C for the Sigma 60 and 7.4 ± 1.0 °C for the Sigma Eye applicators were observed. For the centric focus location, the Sigma 60 showed an average temperature increase of 8.8 ± 0.8 °C, while the Sigma Eye showed 6.8 ± 0.8 °C. For the eccentric focus location, the temperature increase averaged 8.9 ± 0.8 °C for the Sigma 60 and 8.1 ± 1.3 °C for the Sigma Eye. Additional data are provided in Table S2 of Supplementary Materials. Temperature increase per applicator and institution is presented in Figure 6, divided by target location. Except for Sigma Eye applicator at Institution 6, all other applicators fulfilled the minimum requirement of a temperature increase of 6 °C in 10 minutes for both centric and eccentric target locations.

3.2.1.2. Focus location. Focus location was determined for centric target measurements. The results are shown in Figure 7 (Table S2). The data are expressed as the average ± standard deviation for the two radial probes (R1 and R2). Overall, the applicators demonstrated central focusing capability, with average focus locations of 1.5 ± 0.7 cm for Sigma 60 and 1.4 ± 1.2 cm for Sigma Eye. For Institutions 1, 3, and 4, the measured focus was within 1.5 cm of the intended target, while for Institute 2, the measured focus differed approximately 2-2.5 cm. For Sigma Eye at Institution 4, R2 had an error during the mapping procedure, causing a higher deviation. Institution 5 provided data of too low-quality to further assess the obtained value due to malfunctioning of one of the two radial mapping probes (R2).

3.2.1.3. Focus symmetry. The symmetry of the focus (Method 1, using radial probes) for a centric target is presented in Figure 8. It denotes the percentage difference in temperature recorded by each radial probe (R1, R2) at points equidistant from the peak temperature (Figure S4). Ideally, perfect focus symmetry would yield a 0% deviation. Across all institutions and both probes, the average deviation was 3.4 ± 2.5% for the Sigma 60 applicator and 3.1 ± 2.7% for the Sigma Eye applicator, corresponding to an average deviation in temperature of 0.3 ± 0.0 °C for Sigma 60 and 0.2 ± 0.2 °C for Sigma Eye. Additionally, the distance between the peak locations recorded by the two

Table 2. Total number of measurements performed and the number of measurements included in the present study, categorized by institution, applicator, and focus location. The operating frequency of each applicator is also shown.

			Number of measurements			
			Centric target		Eccentric target	
Institution	Applicator	Frequency (MHz)	included	performed	included	performed
Institution 1	Sigma 60	90	3	3	3	3
	Sigma Eye	98	3	3	3	3
Institution 2	Sigma 60	90	3	3	3	3
	Sigma Eye	100	2	3	3	3
Institution 3	Sigma 60	91	2	3	–	–
	Sigma Eye	102	3	5	–	–
Institution 4	Sigma 60	90	1	3	–	–
	Sigma Eye	101	2	2	4	4
Institution 5	Sigma 60	90	–	–	–	–
	Sigma Eye	100	2	3	2	3
Institution 6	Sigma 60	90	1	2	2	2
	Sigma Eye	100	2	3	–	–

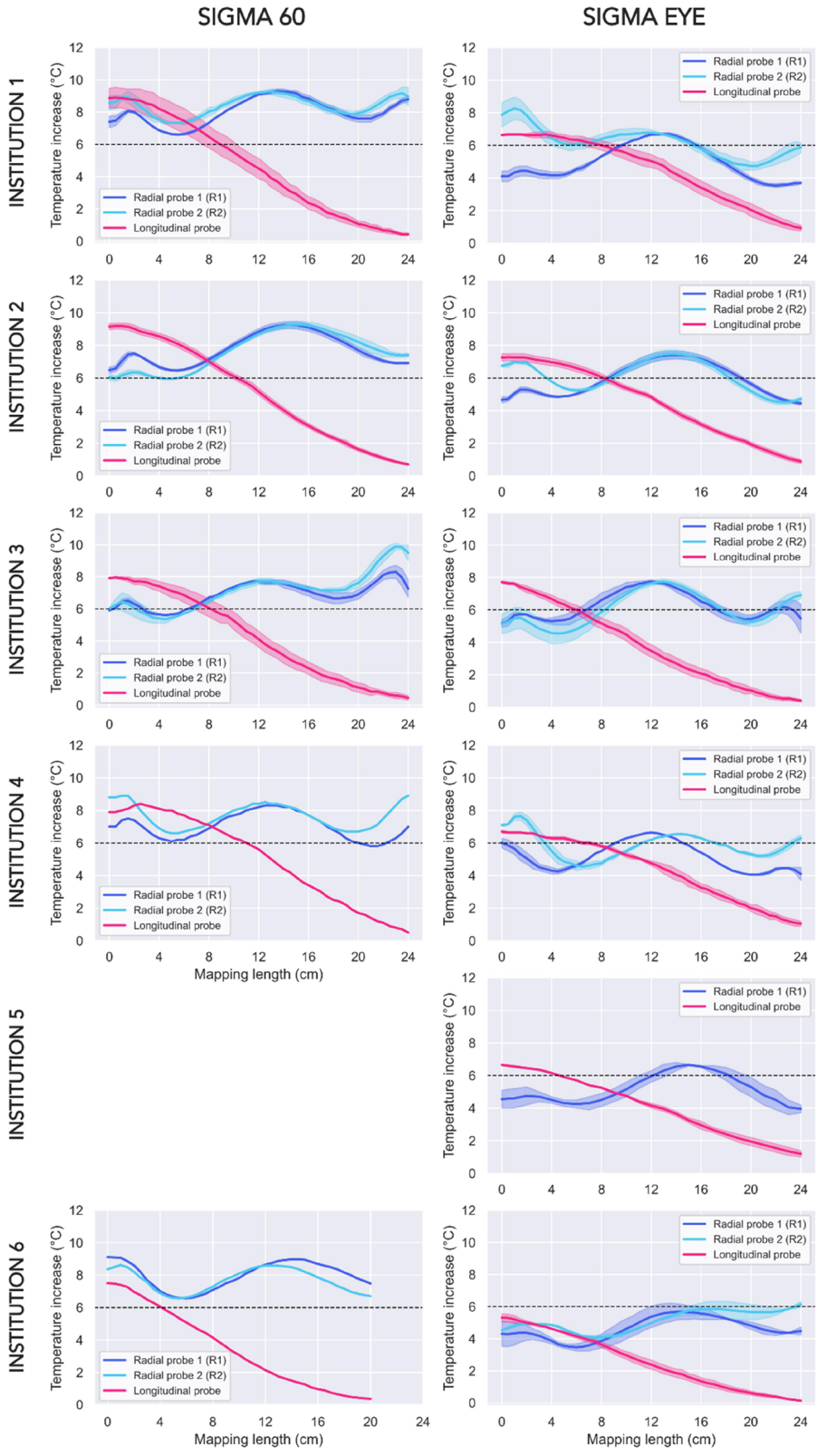

Figure 4. Average (± standard deviation) temperature increase profiles for centric target measurements, shown for each institution (rows) and applicator (columns). Each row represents a different institution. The left column shows data for Sigma 60, while the right column shows data for Sigma Eye. Blue lines represent radial profiles, acquired with radial probes (R1 and R2), while pink lines represent the longitudinal profile acquired from the focus location (x,y) = (0,0) cm. The dashed line represents the minimum temperature increase requirement of 6 °C in 10 minutes. Lines without shading represent single measurements, where no repetitions were available.

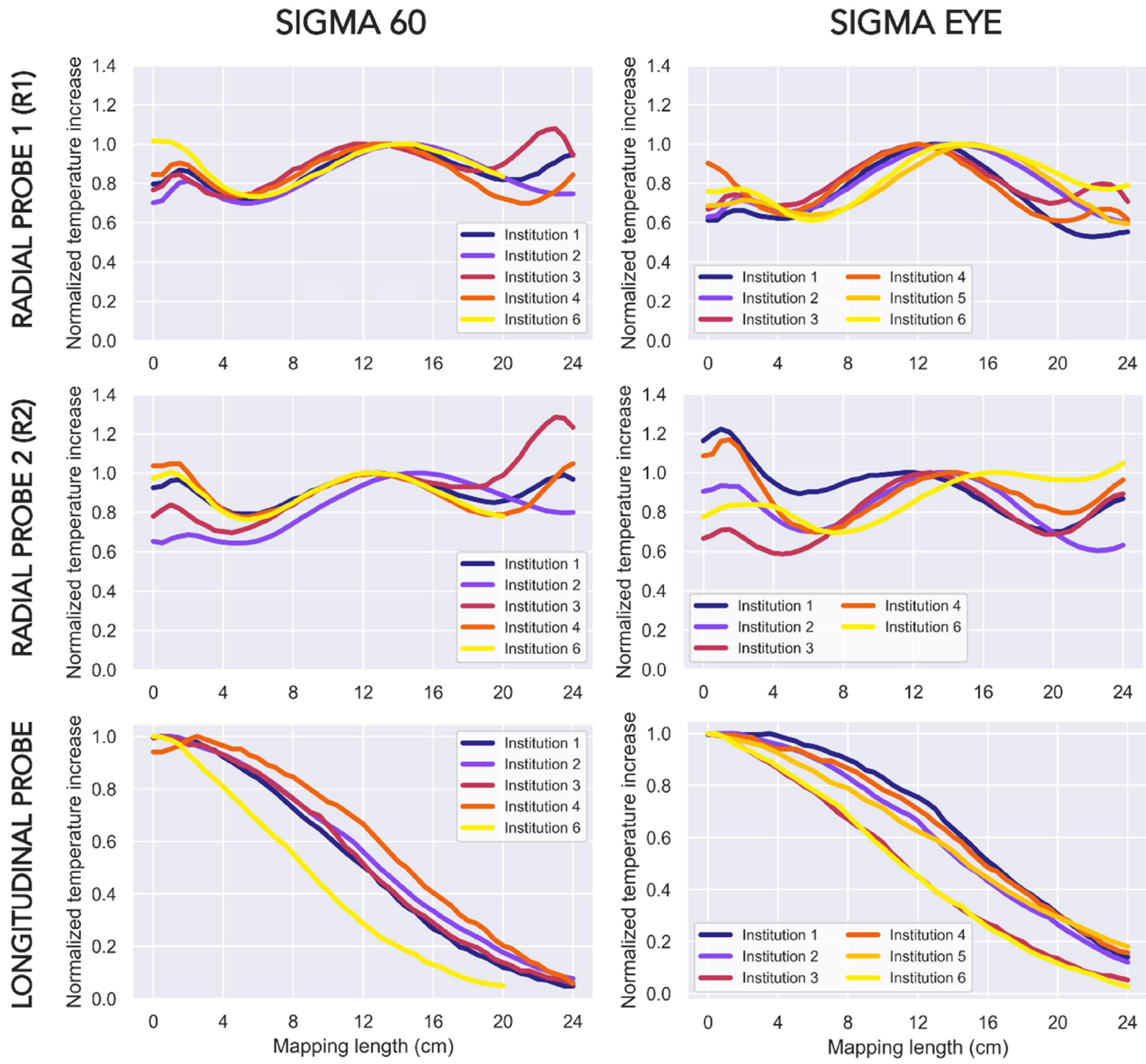

Figure 5. Average centric target profiles, for each institution, for Sigma 60 (left column) and Sigma Eye (right column) applicators, showing normalized temperature increase. Data were normalized to the target maximum value. Each row corresponds to a different probe location: rows one and two represent the radial probes (R1 and R2), while row three represents the longitudinal probe at the target location. Each color represents a different institution.

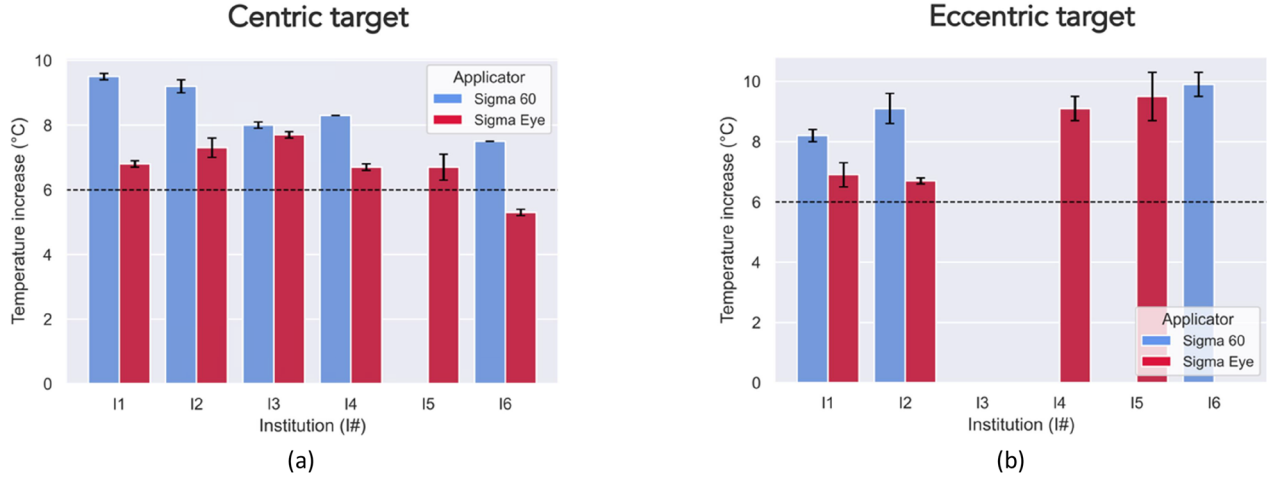

Figure 6. Average temperature increase for centric target (a) and eccentric target (b) per applicator across all institutions, using a set power of 1000 W for 10 minutes. Values represent the mean value ± standard deviation. The dashed line represents the minimum temperature increase requirement.

radial probes was also calculated (in centimeters), averaging 0.7 ± 0.6 cm and 1.1 ± 1.0 cm for Sigma 60 and Sigma Eye applicators, respectively. The results on an institution, applicator and probe basis show that percentage difference in temperature at two points equidistant from the maximum falls within 10%.

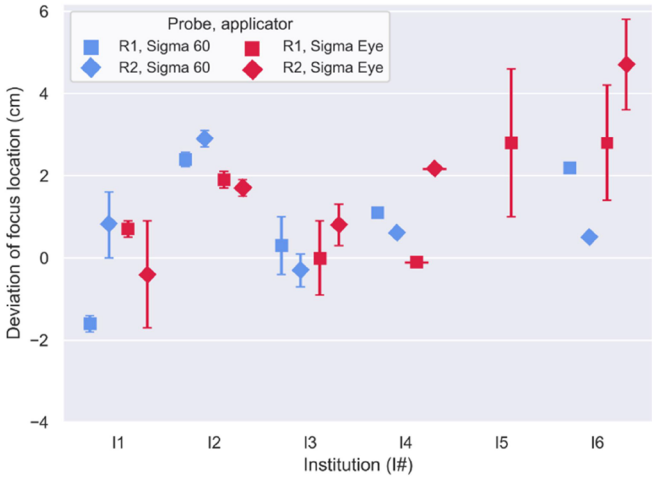

Figure 7. Deviation of focus location from the intended target location (0 cm - centric target) for all institutions, per applicator and per radial probe. (R1: radial probe 1; R2: radial probe 2).

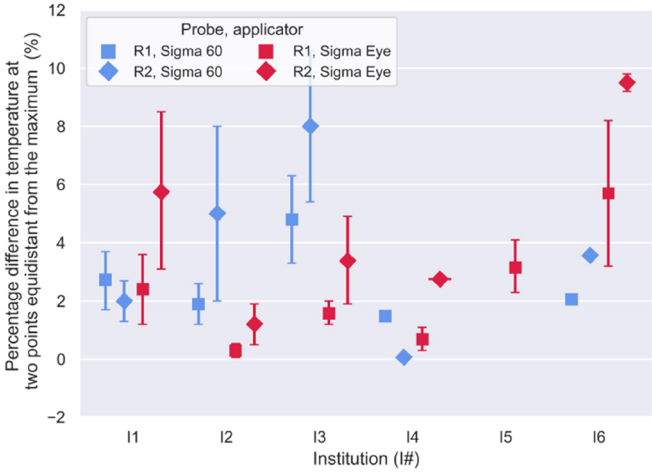

Figure 8. Focus symmetry in terms of percentage difference in temperature between two points equidistant from the maximum value along the radial probes (R1 and R2) for all institutions, per applicator, and per radial probe. (R1: radial probe 1; R2: radial probe 2).

The focus symmetry assessment in Institutions 2 and 3 also includes an evaluation using temperature data recorded at four fixed points (method 2 with longitudinal probes), namely at (6, 0, 0), (-6, 0, 0), (0, -6, 0) and (0, 6, 0), i.e., the (x, y, z) locations in cm. These findings are presented in Table 3, together with the symmetry assessment derived from data collected by the radial probes, considering now a 6 cm distance from the maximum temperature.

4. Discussion

This research presents the first study to systematically design, conduct, and evaluate deep hyperthermia QA measurements using homogeneous phantoms specifically designed to accommodate catheters for temperature monitoring. These temperature measurements were performed using the integrated thermometry systems of the respective deep hyperthermia devices. We evaluated the performance of clinically employed BSD-Sigma 60 and BSD-Sigma Eye applicators across six institutions, assessing various temperature-based quality parameters. Furthermore, this study sought to identify key quality parameters derivable from the acquired data. Practical insights into implementing these procedures in clinical routines are provided, along with valuable guidance for calculating and interpretating of parameters and their respective tolerances.

4.1. QA phantoms

Accurately characterizing deep hyperthermia systems requires tissue-mimicking materials that replicate the properties of human tissues. Thus, verifying the dielectric and thermal properties of these tissue-mimicking mixtures is crucial, ensuring a close match to reference values within an acceptable range of ± 10% [30]. The tissue-mimicking Perfax mixture used in this study falls within this range when compared with muscle tissue dielectric and thermal properties from the most widely used database reporting such parameters, the IT'IS database [29]. Although the permittivity slightly exceeds this threshold, reaching a value of around 75, the heating patterns in the phantom do not significantly change, as shown previously [31]. On the contrary, it leads to sharper temperature gradients. Thermal and dielectric properties of the tissue-mimicking mixture were demonstrated to be stable in time and after repeated heating cycles.

Another critical consideration is ensuring that the phantom design allows for an accurate assessment of the temperature distribution generated by the hyperthermia system. We chose a homogeneous cylindrical phantom for its ease of

Table 3. Focus symmetry in terms of absolute percentage difference (± standard deviation) in temperature evaluated in Institutions 2 and 3, considering the data retrieved from the radial probes (R1 and R2) and the longitudinal probes located at ± 6 cm along the x and y-axes of the central plane of the phantom. R1 and R2 denote the two radial probes, while x and y represent the difference between the probes located ± 6 cm along the x- and y-axes and 0 cm. The corresponding temperature values are reported in parentheses.

Institution	Applicator	Focus symmetry			
		Method 1: radial probes		Method 2: longitudinal probes	
		R1 (%) (°C)	R2 (%) (°C)	x (%) (°C)	y (%) (°C)
2	Sigma 60	3.9 ± 1.0 (0.3 ± 0.1)	9.8 ± 4.1 (0.7 ± 0.3)	12.0 ± 3.3 (0.9 ± 0.2)	13.8 ± 0.8 (1.1 ± 0.0)
3		12.1 ± 4.4 (0.7 ± 0.3)	21.5 ± 6.0 (1.3 ± 0.3)	8.8 ± 10.2 (0.5 ± 0.6)	15.2 ± 4.6 (1.1 ± 0.2)
2	Sigma Eye	0.5 ± 0.1 (0.0 ± 0.0)	4.1 ± 1.7 (0.2 ± 0.1)	5.3 ± 1.9 (0.3 ± 0.1)	12.8 ± 1.9 (0.8 ± 0.1)
3		4.4 ± 0.5 (0.3 ± 0.0)	9.8 ± 5.1 (0.5 ± 0.2)	9.8 ± 6.5 (0.6 ± 1.1)	21.3 ± 2.5 (1.1 ± 0.2)

construction and reproducibility, reduced positioning sensitivity, and enhanced interpretability of results. While more complex phantoms may be suitable for other applications [24,32,33], our choice was guided by these practical advantages. Each homogeneous cylindrical phantom featured 16 strategically positioned catheters capturing temperature distribution and gradients both on the central X-Y plane and longitudinally along the z-axis (Figure 1). The phantom's design, including possible thermal artifacts caused by the plastic catheters on thermal profiles, underwent numerical evaluation as part of a design study [31,34]. This evaluation revealed no significant influence on the temperature profiles.

4.2. QA measurements

The established experimental protocol proved to be both feasible and straightforward, yet careful attention was given to phantom positioning and complete probe insertion. As these factors were appropriately managed, measurements demonstrated reproducibility, evident from the small standard deviations observed within the measurements from each applicator and institute (Figure 4). Figure 4 indicated that the assessed applicators could achieve a temperature increase of 6 °C within a defined area as required by the upcoming QA guidelines, specifically within the intended target region (central). The exception was Institution 6, in which Sigma Eye was not capable of heating more than approximately 5 °C. Several factors could have influenced this result: it is possible to observe that the longitudinal probe did not record the same temperature as radial ones (Figure 4, row 6, column 2), likely because it did not reach the end of the catheter, i.e., the middle of the phantom. Therefore, the maximum temperature might not have been measured.

Quantitative evaluations were mostly performed for centric target measurements. For the focus location, all applicators generated a focus in the center, which means that the focus is within about 1 cm of the middle of the phantom. Nevertheless, deviations from the center location were observed at Institution 4 (Sigma Eye) and Institution 6. While for Institution 4, Sigma Eye (Figure 7) the temperature profile from probe R2 was off, the temperature profile from probe R1 was good. The poor performance of R2 could have been caused by an incorrect location of the R2 probe due to mapping inaccuracies. Thus, the mismatch is derived from mapping errors rather than a focus shift from the center. This reasoning also applies to Sigma 60 at Institution 6. For Sigma Eye of Institution 6, focus deviations were higher. Possible phantom positioning errors explain this. This experiment was the only one performed without the wooden supports, which allowed for reproducible and correct positioning of the phantom in the applicator.

Focus symmetry for centric location was evaluated using two different approaches. The initial approach (Method 1, using radial probes) is based on the data recorded by the radial probes. These results showed asymmetries within 10% for all institutions (Figure 8), corresponding to temperature differences up to approximately 0.6 °C (Table S2). For two institutions, we compared Method 1 (radial probes), using a value of 6 cm, and Method 2 (longitudinal probes). The values obtained with the two methods do not exhibit a clear relation (Table 3). Method 2 (using longitudinal probes) seems to yield greater differences than Method 1. One of the main reasons is related to the assumptions of Method 2: it assumes that the heating is precisely focused at the center of the phantom. In cases where deviations are present, the temperature recorded by some of the symmetric four longitudinal probes will automatically be higher or lower than that recorded by the others. When adopting method 1 (radial probes), symmetry is calculated with respect to the maximum temperature peak for each of the radial probes, which reduces the impact of a potentially shifted focus. However, it is much more sensitive to spatial accuracy since it is based on multiple points recorded along the catheter track. For future evaluation, we recommend method 1 (radial probes) for symmetry analysis.

4.3. Recommendation thresholds for QA measurements

Recommendations and thresholds should be based on evidence and practical experience to account for systems and experimental inaccuracies. The accuracy of hyperthermia systems depends on phase and amplitude measurements from the radiofrequency-control device, matching, and crosstalk of individual antennas, among others factors. The manufacturer specifies a phase accuracy tolerance of ± 10° per channel for the evaluated system. If we consider the average permittivity of the phantom (ε_r = 74.4), this translates to a potential focus shift of ± 2 cm in both the x and y directions when using the Sigma 60 applicator, considering the combined uncertainty of ± 20° from two channels controlling the shifts in each direction. Moreover, thermal probes occasionally became stuck, resulting in skewed or artificially constant temperature readings over a few centimeters (e.g., the longitudinal probe at Institution 1, Sigma Eye). The automatic mapping process sometimes failed and contributed to deviations of up to 2 cm between radial probes, which would shift the resulting temperature profiles. To mitigate this problem, we propose verifying the thermal mapping performance through a dry run in marked transparent catheters. Combining the previous factors, we recommend a maximum error of 2 cm for the focus location parameter.

For temperature measurements, an inaccuracy of ± 0.2 °C is expected for the thermal probes used, as stated by the manufacturer [20]. This affects both the assessment of temperature increase and the evaluation of focus symmetry. Additionally, when assessing the maximum temperature increase achieved by the applicator, the correct positioning of the probe relative to the center of the applicator significantly impacts the recorded values. We determined that an offset of up to 6 mm in the longitudinal positioning of the probe results in a deviation of ± 0.2 °C. Therefore, we propose an acceptable deviation of ± 0.4 °C for recorded temperature increases using longitudinal probes.

Regarding focus symmetry, asymmetries within 10% were observed in most institutions when applying Method 1 (radial probes). However, this approach must account for the inaccuracy of probe positioning, which, as mentioned earlier, can lead to an average spatial accuracy of ± 2.0 cm for the mapping system. Considering this, along with the thermal probe's measurement accuracy, we recommend a threshold of 10% for this method, which corresponds to a temperature deviation of up to 0.6 °C. For Method 2 (longitudinal probes), the impact of mapping inaccuracy is excluded, although there may still be some uncertainty in the probe's positioning relative to the applicator's central plane. However, this has a limited impact, with a deviation of up to 0.2 °C. Therefore, we

Table 4. Quality assurance parameters evaluated, number of probes used, corresponding measurement setup, and recommended tolerances. Recommended tolerances are based on performed measurements and respective uncertainties. Note that the target size shown in the image does not reflect the actual focus size; it is only a graphical representation.

	Target	Number of probes	Setup	Recommended tolerances
Temperature increase	Centric/Eccentric	1 longitudinal probe in the target location	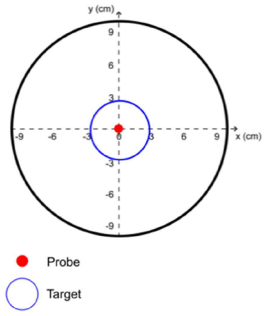	6 °C in 10 min ±0.4 °C
Focus location	Centric	2 axial probes 3 longitudinal probes	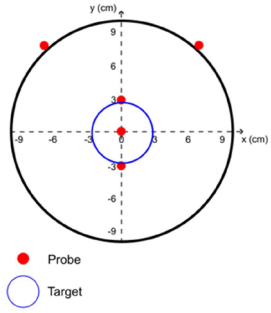	< ±2.0 cm
	Eccentric	2 axial probes 3 longitudinal probes	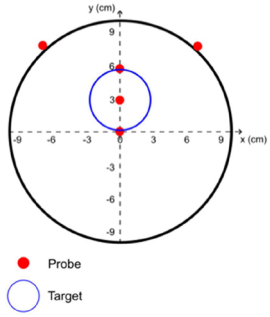	< ±2.0 cm
Focus symmetry	Centric	Method 1 2 axial probes 1 longitudinal probe	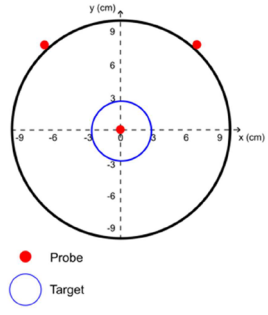	≤ 10% (≤ ±0.8 °C)
		Method 2 5 longitudinal probes	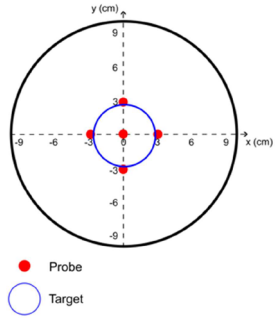	≤ 10 % (≤ ±1 °C)

ommend a threshold of 10% for this method, limiting the corresponding temperature deviation to below 1 °C.

Based on all of these, we recommend the QA parameters, setups, and corresponding thresholds listed in Table 4.

4.4. Limitations

All ESHO QA guidelines are designed from an intra-institutional perspective, which reduces variability in equipment performance and measurement protocols when comparing QA measurements within a single institution. However, the study reported here involves significantly greater variability in equipment performance, including factors such as heating efficiency, temperature and mapping accuracy. As a result, these findings offer important insights into the challenges associated with conducting inter-institutional assessments and comparing the QA performance of an existing and widely used deep hyperthermia device. In this section, we highlight several limitations that must be addressed to ensure the successful implementation of multi-institutional QA comparisons.

All measurements were conducted over a period of approximately three weeks, with two days allocated to each institution visited. Medical physicists and engineers at each institution were informed about the planned measurements, providing them and the manufacturer time to verify and test the equipment in advance, should any issues arise. Ideally, many of the probe-related issues encountered could have been identified and resolved before the experiments began. To further improve temperature accuracy, an additional step would have been to calibrate all probes using the same water bath and reference sensor at each institution. Although this was not feasible during our measurements, it is strongly recommended for future studies involving multiple institutions.

Data analysis was performed only after the completion of all measurements, which prevented any adjustments or improvements from being implemented during the measurement phase. Therefore, we propose the following recommendations to improve future measurements and testing procedures. For evaluating the centric focus location, we recommend using five probes, as shown in Table 4, instead of just two radial probes as employed in this study. The rationale is that the data points from the additional three longitudinal probes provide multiple measurement points along the same axis, allowing for curve fitting to determine the location of the maximum temperature. Furthermore, the two radial curves can be combined with the first to yield a more accurate estimate of the focus location. The procedure for evaluating the location of steering targets is similar. Temperature measurements should be taken along the three longitudinal catheters in the axis where the target is positioned—specifically along one of the two main axes of the phantom (x or y). We recommend steering the focus to (x, y) = (0, 3) cm and positioning the probes at (x, y) coordinates of (0, 0), (0, 3), and (0, 6) cm. This approach minimizes potential interference from the phantom's plastic wall associated with a (x, y) = (0, 6) cm target, while providing a clinically relevant target location. Physicists from multiple institutions have noted that target locations are often shifted 3-4 cm from the center rather than 6 cm. The data points from the three longitudinal probes can be used for curve fitting along the y-axis, while additional curves can be fitted using the data from radial probes positioned at $y = 3$ cm. Combining these three fitted curves will help estimate the focus location more accurately. We were not able to follow these procedures (Table 4) since most institutions had only three temperature probes available. In those cases, an alternative approach is to steer the focus to the same x, y values, e.g., (x, y) = (3, 3) cm, or rotate the phantom to have one of the radial catheters passing in the location of the steered focus of (x, y) = (0, 3) cm.

Finally, measurements were only performed for the BSD-family systems, meaning single-brand systems. Therefore, some of the recommended thresholds and thermometry issues might not be applicable for other devices. Nevertheless, phantom design, QA measurements, and quantitative parameters should be applicable across all hyperthermia systems, while the threshold should be an indication, and if needed, modifications should be done. The latter illustrates the need to strictly implement the QA guidelines to enable inter-institutional comparison of the existing hyperthermia systems on their performance.

5. Conclusions

This study presented and analyzed a representative series of temperature measurements conducted across various hyperthermia institutions. Several QA parameters were estimated and compared both within and across all institutions. We found that all but one applicator achieved the required temperature increase of 6 °C within 10 minutes, a fundamental criterion for hyperthermia heating devices. Additionally, all applicators successfully generated a clear central focus within approximately 1 cm of the phantom's center, with asymmetries up to 10% (0.8 °C).

Despite these generally favorable results, our multi-institutional QA study uncovered minor issues indicating that institutions performing hyperthermia may underestimate the importance of applying consistent QA standards to enable reliable inter-institutional comparisons. To address this, we propose regular QA measurements to follow the implementation and recommendations presented here. Further, we derived and presented minimum acceptable values for the different parameters, taking into account uncertainties from the equipment (e.g., phase and amplitude inaccuracies, cross-coupling, and thermal mapping) and operational errors, such as probe and phantom positioning. These findings, along with the phantom design and measurement recommendations, aim to facilitate the consistent implementation of QA experiments for deep hyperthermia systems.

Acknowledgments

The authors would like to thank all the people involved in the experimental processes at the six visited institutes, namely Manfred Schmidt from Department of Radiation Oncology, University Hospital, Erlangen, Erlangen, Germany; Ulf Lamprecht from Department of Radiation Oncology, University Hospital Tübingen, Tübingen, Germany; Marianne Goeger-Neff and Sultan Abdel-Rahman from Department of Medicine III, University Hospital, LMU Munich, Munich, Germany; Jacek Nadobny and Pirus Ghadjar from Department of Radiation Oncology, Charité - Universitätsmedizin Berlin, Freie Universität Berlin, Humboldt-Universität

zum Berlin, and Berlin Institute of Health, Berlin, Germany; Oliver Mils and Ruediger Wessalowski from Department of Pediatric Hematology, Oncology and Clinical Immunology, Medical Faculty, Heinrich-Heine-University Düsseldorf, Düsseldorf, Germany; Abdelali Ameziane, Anderson Cruz Perdomo from Department of Radiotherapy, Erasmus MC Cancer Institute, University Medical Center Rotterdam, Rotterdam, the Netherlands. Additionally, the authors would like to acknowledge Hans Crezee and Dario Rodrigues for fruitful discussions.

Disclosure statement

No potential conflict of interest was reported by the authors.

Funding

This research has received support from the European Union's Horizon 2020 research and innovation program under the Marie Skłodowska-Curie (MSCA-ITN) grant 'Hyperboost' project, no. 955625.

ORCID

Mattia De Lazzari http://orcid.org/0000-0002-9736-5457
Dietmar Marder http://orcid.org/0000-0003-0865-9283
Gerard C. van Rhoon http://orcid.org/0000-0002-7365-5783
Sergio Curto http://orcid.org/0000-0002-3073-1117
Hana Dobšíček Trefná http://orcid.org/0000-0001-6025-0819

Data availability statement

Raw data were gathered from the six different institutions included in this study. Derived data and code supporting the findings presented in this study are available from the corresponding author M.L. on request.

References

[1] Oei AL, Kok HP, Oei SB, et al. Molecular and biological rationale of hyperthermia as radio-and chemosensitizer. Adv Drug Deliv Rev. 2020;163-164:84–97. doi: 10.1016/j.addr.2020.01.003.
[2] Horsman M, Overgaard J. Hyperthermia: a potent enhancer of radiotherapy. Clin Oncol (R Coll Radiol). 2007;19(6):418–426. doi: 10.1016/j.clon.2007.03.015.
[3] Lutgens L, van der Zee J, De Ruysscher DKM, et al. Combined use of hyperthermia and (chemo)radiation therapy for treating locally advanced cervix carcinoma. Cochr Database Syst Rev. 2010;(3):CD006377. doi: 10.1002/14651858.CD006377.pub3.
[4] Datta NR, Ordóñez SG, Gaipl US, et al. Local hyperthermia combined with radiotherapy and-/or chemotherapy: recent advances and promises for the future. Cancer Treat Rev. 2015;41(9):742–753. doi: 10.1016/j.ctrv.2015.05.009.
[5] Peeken JC, Vaupel P, Combs SE. Integrating hyperthermia into modern radiation oncology: what evidence is necessary? Front Oncol. 2017;7:132. doi: 10.3389/fonc.2017.00132.
[6] Wust P, Hildebrandt B, Sreenivasa G, et al. Hyperthermia in combined treatment of cancer. Lancet Oncol. 2002;3(8):487–497. doi: 10.1016/s1470-2045(02)00818-5.
[7] Issels R, Kampmann E, Kanaar R, et al. Hallmarks of hyperthermia in driving the future of clinical hyperthermia as targeted therapy: translation into clinical application. Int J Hyperthermia. 2016;32(1):89–95. doi: 10.3109/02656736.2015.1119317.
[8] van der Zee J, González González D, van Rhoon GC, et al. Comparison of radiotherapy alone with radiotherapy plus hyperthermia in locally advanced pelvic tumours: a prospective, randomised, multicentre trial. Lancet. 2000;355(9210):1119–1125. doi: 10.1016/s0140-6736(00)02059-6.
[9] Issels RD, Lindner LH, Verweij J, et al. Neo-adjuvant chemotherapy alone or with regional hyperthermia for localised high-risk soft-tissue sarcoma: a randomised phase 3 multicentre study. Lancet Oncol. 2010;11(6):561–570. doi: 10.1016/S1470-2045(10)70071-1.
[10] van Driel WJ, Koole SN, Sikorska K, et al. Hyperthermic intraperitoneal chemotherapy in ovarian cancer. N Engl J Med. 2018;378(3):230–240. doi: 10.1056/NEJMoa1708618.
[11] Hurwitz MD. Hyperthermia and immunotherapy: clinical opportunities. Int J Hyperthermia. 2019;36(sup1):4–9. doi: 10.1080/02656736.2019.1653499.
[12] Franckena M, Fatehi D, de Bruijne M, et al. Hyperthermia dose-effect relationship in 420 patients with cervical cancer treated with combined radiotherapy and hyperthermia. Eur J Cancer. 2009;45(11):1969–1978. doi: 10.1016/j.ejca.2009.03.009.
[13] Kroesen M, Mulder HT, van Holthe JML, et al. Confirmation of thermal dose as a predictor of local control in cervical carcinoma patients treated with state-of-the-art radiation therapy and hyperthermia. Radiother Oncol. 2019;140:150–158. doi: 10.1016/j.radonc.2019.06.021.
[14] Bakker A, Tello Valverde CP, van Tienhoven G, et al. Post-operative re-irradiation with hyperthermia in locoregional breast cancer recurrence: temperature matters. Radiother Oncol. 2022;167:149–157. doi: 10.1016/j.radonc.2021.12.036.
[15] Dewhirst MW, Phillips TL, Samulski TV, et al. RTOG quality assurance guidelines for clinical trials using hyperthermia. Int J Radiat Oncol Biol Phys. 1990;18(5):1249–1259. doi: 10.1016/0360-3016(90)90466-w.
[16] Lagendijk JJ, Van Rhoon GC, Hornsleth SN, et al. ESHO quality assurance guidelines for regional hyperthermia. Int J Hyperthermia. 1998;14(2):125–133. doi: 10.3109/02656739809018219.
[17] Bruggmoser G, Bauchowitz S, Canters R, et al. Quality assurance for clinical studies in regional deep hyperthermia. Strahlenther Onkol. 2011;187(10):605–610. doi: 10.1007/s00066-011-1145-x.
[18] Bruggmoser G. Some aspects of quality management in deep regional hyperthermia. Int J Hyperthermia. 2012;28(6):562–569. doi: 10.3109/02656736.2012.714049.
[19] Trefná HD, Crezee H, Schmidt M, et al. Quality assurance guidelines for superficial hyperthermia clinical trials: I. Clinical requirements. Int J Hyperthermia. 2017;33(4):471–482. doi: 10.1080/02656736.2016.1277791.
[20] Dobšíček Trefná H, Crezee J, Schmidt M, et al. Quality assurance guidelines for superficial hyperthermia clinical trials: II. Technical requirements for heating devices. Strahlenther Onkol. 2017;193(5):351–366. doi: 10.1007/s00066-017-1106-0.
[21] Dobšíček Trefná H, Schmidt M, van Rhoon GC, et al. Quality assurance guidelines for interstitial hyperthermia. Int J Hyperther. 2019;36(1):276–293. doi: 10.1080/02656736.2018.1564155.
[22] Wust P, Stahl H, Löffel J, et al. Clinical, physiological and anatomical determinants for radiofrequency hyperthermia. Int J Hyperthermia. 1995;11(2):151–167. doi: 10.3109/02656739509022453.
[23] Mulder HT, Curto S, Paulides MM, et al. Systematic quality assurance of the BSD2000-3D MR-compatible hyperthermia applicator performance using MR temperature imaging. Int J Hyperthermia. 2018;35(1):305–313. doi: 10.1080/02656736.2018.1497209.
[24] Curto S, Aklan B, Mulder T, et al. Quantitative, multi-institutional evaluation of MR thermometry accuracy for deep-pelvic MR-hyperthermia systems operating in multi-vendor MR-systems using a new anthropomorphic phantom. Cancers (Basel). 2019;11(11):1709. doi: 10.3390/cancers11111709.
[25] La Gioia A, Porter E, Merunka I, et al. Open-ended coaxial probe technique for dielectric measurement of biological tissues: challenges and common practices. Diagnostics. 2018;8(2):40. doi: 10.3390/diagnostics8020040.
[26] Silva NP, Bottiglieri A, Conceição RC, et al. Characterisation of ex vivo liver thermal properties for electromagnetic-based hyperthermic therapies. Sensors. 2020;20(10):3004. doi: 10.3390/s20103004.
[27] Farina L, Sumser K, van Rhoon G, et al. Thermal characterization of phantoms used for quality assurance of deep hyperthermia systems. Sensors (Basel). 2020;20(16):4549. doi: 10.3390/s20164549.

[28] Turner P, Tumeh A, Schaefermeyer T. BSD-2000 approach for deep local and regional hyperthermia: physics and technology. Strahlenther Onkol. 1989;165(10):738–741.
[29] Hasgall PA, Baumgartner DGF, Neufeld C, et al. IT'IS Database for thermal and electromagnetic parameters of biological tissues. 2022.
[30] Schneider C, Olmi R, Van Dijk J. Phantom design: applicability and physical properties, in thermoradiotherapy and thermochemotherapy: biology, physiology, physics. Berlin (Heidelberg): Springer; 1995. p. 381–397.
[31] Rodrigues D. Phantom design for thermometry-based quality assurance of deep hyperthermia applicators. ICHO. Digital. 2021.
[32] Gellermann J, Wlodarczyk W, Ganter H, et al. A practical approach to thermography in a hyperthermia/magnetic resonance hybrid system: validation in a heterogeneous phantom. Int J Radiat Oncol Biol Phys. 2005;61(1):267–277. doi: 10.1016/j.ijrobp.2004.05.009.
[33] Dabbagh A, Abdullah BJJ, Abu Kasim NH, et al. Reusable heat-sensitive phantom for precise estimation of thermal profile in hyperthermia application. Int J Hyperthermia. 2014;30(1):66–74. doi: 10.3109/02656736.2013.854930.
[34] De Lazzari M. Design and manufacture procedures of phantoms for hyperthermia QA guidelines. EuCAP 2023: Florence. 2023.